International Journal of Thermal Sciences 89 (2015) 34–42

Contents lists available at ScienceDirect

International Journal of Thermal Sciences

journal homepage: www.elsevier.com/locate/ijts

3D numerical study on shell side heat transfer and flow characteristics of rod-baffle heat exchangers with spirally corrugated tubes

J.J. Liu, Z.C. Liu, W. Liu*

School of Energy and Power Engineering, Huazhong University of Science and Technology, Wuhan 430074, China

A R T I C L E I N F O

Article history:
Received 4 March 2014
Received in revised form
18 October 2014
Accepted 18 October 2014
Available online 14 November 2014

Keywords:
Rod-baffle heat exchanger
Spirally corrugated tube
Heat transfer enhancement
Numerical simulation
Physical quantity synergy

A B S T R A C T

This article presents a numerical simulation of the shell side flow in rod-baffle heat exchangers with spirally corrugated tubes (RBHXsSCT). Results are compared with those in rod-baffle heat exchanger with plain tubes (RBHX). Simulation is conducted to improve the thermo–hydraulic performance in longitudinal flow heat exchangers and to obtain an understanding of the physical behavior of thermal and fluid flow in the RBHXsSCT with Reynolds number ranging from 6000 to 18,000. Simulation results show that the Nusselt number in RBHXSCT with one-start spirally corrugated tubes can be 1.2 times that in RBHX when the Reynolds number is 18,000. The heat transfer quantities in the RBHXsSCT with one-start, two-start, three-start, and four-start spirally corrugated tubes are 104.6%, 105.4%, 106.7%, and 109.6%, respectively, higher than that in RBHX. The pressure drop in RBHX is 1.21, 1.16, 1.12, and 1.08 times that in RBHXsSCT with one-start, two-start, three-start, and four-start spirally corrugated tubes, respectively. The RBHXSCT with one-start spirally corrugated tubes can achieve an efficiency evaluate coefficient of 1.35. Physical quantity synergy analysis is performed to investigate heat transfer and flow resistance performance. Results verify the synergy regulation among the physical quantities of fluid particle in the flow field of the convective.

1. Introduction

Shell-and-tube heat exchangers (STHXs) are extensively used in petroleum refining, chemical engineering, and power generation, among others [1]. The fluid flow in STHXs can be divided into tube side flow and shell side flow. A large amount of heat–transfer enhancement techniques, such as rectangular tubes and tube inserts [2–11], have been developed and applied in the tube side of the STHXs to save energy. Meanwhile, the performance of the shell side is mainly dependent on the flow status in STHXs. The heat transfer rate is relatively high in cross flow heat exchangers, such as the segmental–baffle shell–tube heat exchangers [12–20]. However, the pressure drop and the "dead" flow region are extremely large, and harmful vibrations are violent. The longitudinal flow heat exchangers have the following advantages compared with the cross flow heat exchangers: (1) considerable reduction of the pressure drop and the pump power loss in the shell sides; (2) avoidance of the vibrations and security enhancement of heat exchangers; (3) decrease of "dead" flow regions and generation of fouling and corrosion [1]. Therefore, as typical longitudinal flow heat exchangers, the rod-baffle heat exchangers (RBHXs), which were originally proposed in the 1970s by Phillips Petroleum Company [21–23], have been extensively studied by researchers because of the above mentioned advantages.

Smyth [24] conducted an experimental study on RBHXs. The results showed that in the RBHXs, the heat transfer coefficients slightly increased, and the pressure loss significantly decreased compared with the traditional STHXs, leading to reduced cost of exchangers and in some instances smaller exchangers. Ma et al. [25] analyzed the flow and heat transfer characteristics on the combinations of rod baffle with different types and distances by numerical simulation on the basis of RBHXs. The simulation results indicated that the rod baffle type of ellipse as well as the rod baffle distance of 120 mm showed the best performance. Ma et al. [26] designed a new type of RBHX, which has variable sections to optimize the heat exchanger. The results indicated that the comprehensive performance of the variable section RBHX increased by 13%–14% than the uniform section RBHX. Dong et al. [27] adopted a unit duct model to analyze the influence of the rod baffle on the flow of the shell side and to present the status of turbulent flow and heat transfer in the shell side of the STHX with rod baffle. The simulation results showed that the rod baffles placed vertically and horizontally in the unit duct continuously sheared

* Corresponding author. Tel.: +86 27 87541998; fax: +86 27 87540724.
E-mail address: w_liu@hust.edu.cn (W. Liu).

http://dx.doi.org/10.1016/j.ijthermalsci.2014.10.011
1290-0729/

and comminuted the streamlines of the flow when the fluid crosses over the rod-baffles, change the fluid flow directions, and result in the disruption of the continuity and stability of the fluid. Wang [28] proposed and investigated a new type of RBHX with thick and thin rods on the basis of the principle of heat transfer enhancement in the core flow [29]. The results presented that with the combined structure. The heat transfer presented no significant degradation, but the flow resistance can be reduced; thus significantly improving the overall performance.

From the foregoing reviews, we found that few studies focused on changing the types of heat exchanger tubes in RBHX to improve the thermal-hydraulic characteristics of the shell side. In this paper, we put forward the RBHX with spirally corrugated tubes (RBHXsSCT) aiming at improving the overall thermal performance of the shell sides compared with the RBHXs. The numerical simulation method is adopted to visualize the flow region and to predict the thermal–hydraulic performance because the numerical simulation is cheaper and more time–saving compared with the experimental study [30–34]. The 3D numerical simulations with whole models of RBHXsSCT and RBHXs are presented to investigate the heat transfer performances and flow resistance characteristics on the shell side by using the commercial software of FLUNET 14.0 with grid systems generated by ICEM–CFD. The principle of physical quantity synergy [35–38] is used to discuss the thermal–hydraulic performance of RBHXsSCT.

2. Model for whole heat exchanger simulation

2.1. Computational model

The computational models of RBHXSCT and RBHX are shown in Fig. 1, and the numerical simulation is conducted only on the shell side of the heat exchangers. The geometry parameters are listed in Table 1. As shown in Fig. 1 21 heat exchanger tubes are present in each heat exchanger and are in square arrangement. Water is selected as the working fluid.

The following assumptions are made to simplify the numerical simulations: (1) the thermal–physical properties of fluid such as ρ, μ, c_p, λ are constant; (2) fluid is incompressible, isotropic, and continuous; (3) the effect of gravity is negligible; (4) the flow state is steady.

2.2. Numerical simulation method

The general control equation for convective heat transfer is expressed as follows:

$$\mathrm{div}(\rho U\phi) = \frac{\partial}{\partial x}\left(\Gamma\frac{\partial\phi}{\partial x}\right) + \frac{\partial}{\partial y}\left(\Gamma\frac{\partial\phi}{\partial y}\right) + \frac{\partial}{\partial z}\left(\Gamma\frac{\partial\phi}{\partial z}\right) \quad (1)$$

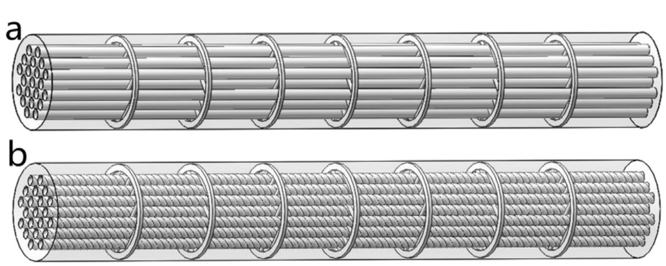

Fig. 1. The model of different heat exchangers. (a) Rod-baffle heat exchanger with plain tubes. (b) Rod-baffle heat exchanger with spirally corrugated tubes.

Table 1
The geometry parameters of whole model.

Item	Values
Shell-side parameters	
D (mm)	144
Shell-side length (mm)	1000
Rod parameters	
p_r (mm)	5.5
Rod pitch in each baffle (mm)	22
Baffle parameters	
Thickness (mm)	5
Baffle pitch (mm)	120
Spirally corrugated tube parameters	
d_s (mm)	16
Groove depth (mm)	3
Start numbers	1–4
Plain tube parameters	
d_0 (mm)	16

where ρ is the fluid density; U is fluid velocity vector; Γ is the generalized diffusion coefficient. For continuity equation, $\phi = 1$; for momentum equation, ϕ is velocity vector; and for energy equation, $\phi = T$.

The standard k–ε two-equation model is adopted for the turbulent region, and the two equations are expressed as follows:

$$\frac{\partial(\rho U_i k)}{\partial x_i} = \frac{\partial}{\partial x_j}\left[\left(\mu + \frac{\mu_t}{\sigma_k}\right)\frac{\partial k}{\partial x_j}\right] + G_k + G_b - \rho\varepsilon - Y_M + S_k \quad (2)$$

$$\frac{\partial(\rho U_i \varepsilon)}{\partial x_i} = \frac{\partial}{\partial x_j}\left[\left(\mu + \frac{\mu_t}{\sigma_\varepsilon}\right)\frac{\partial \varepsilon}{\partial x_j}\right] + C_{1\varepsilon}\frac{\varepsilon}{k}\left(G_k + C_{3\varepsilon}G_b\right) - C_{2\varepsilon}\rho\frac{\varepsilon^2}{k} + S_\varepsilon \quad (3)$$

where k is the turbulent kinetic energy; ε is the turbulent dissipation rate; G_k is the producing item of k engendered by the average velocity gradient; G_b is the producing item of k engendered by buoyancy; Y_M is the contribution term from turbulent pulse expansion; $C_{1\varepsilon}$, $C_{2\varepsilon}$, $C_{3\varepsilon}$ are empirical constants; σ_k and σ_ε are Prandtl numbers corresponding to k and ε; S_k and S_ε are user-defined source terms.

We then present the boundary conditions. The non–slip boundary condition is applied on all solid surfaces. The standard wall function method is used to simulate flow in the near-wall region. The surfaces of solid regions, rod-baffles, and inner wall of the shell side are set as adiabatic because the heat exchangers are well insulated and the heat loss to surroundings is neglected. The velocity inlet and outflow boundary condition are applied for the inlet and outlet, respectively, because fluid is incompressible. The temperatures of the tube wall and inlet fluid are set as constant, which are 330 and 300 K, respectively. The shell wall and rod-baffle surface are set as adiabatic. The finite volume method and the second-order upwind difference scheme are applied, and the SIMPLEC algorithm is adopted for the coupling between pressure and velocity field. The second-order upwind difference scheme is applied for energy and momentum computation, and the standard

Table 2
Thermo-physical properties of water.

Parameter	Value
c_p (J/kg K)	4182
μ (kg/m s)	0.001003
ρ (kg/m^3)	998.2
λ (W/m K)	0.6

difference scheme is used for pressure computation. Water is set as working fluid, and the parameters are given in Table 2.

The 3D grid system was generated by using the commercial software ICEM CFD14.0 on the basis of the 3D geometry created in a commercial CAD program. The computational domain is discretized with unstructured tetrahedral elements, and the regions adjacent to the tubes and the rods are meshed better to meet the requirement of the wall function method. The meshes of the computational model are shown in Fig. 2. Grid independence tests are carried out to ensure that the grid independent solution can be obtained. The results of the grids independent test are shown in Table 3. From the test values of the Nusselt numbers and the pressure drop obtained by the four grid systems, the 3.6×10^7 grid system is found to be dense enough to result in grid-independent solutions. Accordingly, the grid system with 3.6×10^7 grids is employed to perform the following calculations, and the present numerical predictions have reasonable accuracy. The commercial software Fluent 14.0 is adopted for computational fluid dynamics method, and all numerical simulations are performed on workstations with 20 dual–core CPUs and 240 GB RAM. Every simulation case takes 24 h to obtain the converged solutions approximately.

The paper [40] provides the comparisons of shell-side whole modeling in RBHXs approach on predicting heat transfer and pressure drop with experimental method. In this paper, the maximum discrepancies are about 10.8% for Nusselt number and 12.4% for pressure drop. Therefore it is decided that the whole modeling approach has a high precision on predicting thermal-hydraulic performance.

2.3. Data reduction

The Reynolds number of the shell side is expressed as follows:

$$\mathrm{Re} = \frac{\rho u D_e}{\mu} \tag{4}$$

where u is the inlet average velocity of the shell side; ρ is the fluid density; μ is the coefficient of dynamic viscosity; D_e is the equivalent diameter, which is expressed as follows:

$$D_{e(\mathrm{RBHX})} = \frac{4A_0}{P_0} = \frac{\pi \cdot D^2 - \pi \cdot n \cdot d_0^2}{\pi \cdot D + \pi \cdot n \cdot d_0} \tag{5}$$

$$D_{e(\mathrm{RBHXSCT})} = \frac{4A_s}{P_s} = \frac{\pi \cdot D^2 - 4 \cdot n \cdot a_{\mathrm{sct}}}{\pi \cdot D + n \cdot p_{\mathrm{sct}}} \tag{6}$$

Here, $D_{e(\mathrm{RBHx})}$ and $D_{e(\mathrm{RBHxST})}$ are the equivalent diameter of RBHX and RBXHSCT; A_0 and A_s are the sectional area of RBHX and RBXHSCT; P_0 and P_s are the sectional wetting perimeter of RBHX and RBXHSCT; a_{sct} is the sectional area of the spirally corrugated tube in RBHSSCT; p_{sct} is the perimeter of the spirally corrugated tube; n is the number of tubes.

Table 3
Influence of the grid numbers on the computed result.

Grid number	ΔNu	Δp
9.3×10^6 to 2.9×10^7	17%	11%
2.9×10^7 to 3.6×10^7	4.8%	3.9%
3.6×10^7 to 4.3×10^7	2.2%	2.8%

For the readers' convenience, the major equations on heat transfer are shown as follows:

$$Q = M \cdot c_p \cdot (t_{\mathrm{out}} - t_{\mathrm{in}}) \tag{7}$$

$$h = \frac{Q}{S \cdot \Delta t_m} \tag{8}$$

$$\Delta t_m = \frac{\Delta t_{\max} - \Delta t_{\min}}{\ln(\Delta t_{\max}/\Delta t_{\min})} \tag{9}$$

$$\Delta t_{\max} = t_{\mathrm{wall}} - t_{\mathrm{in}} \tag{10}$$

$$\Delta t_{\min} = t_{\mathrm{wall}} - t_{\mathrm{out}} \tag{11}$$

$$\mathrm{Nu} = \frac{h \cdot D_e}{\lambda} \tag{12}$$

3. Simulation results and discussions for the models of RBHXsSCT and RBHX

3.1. Flow structure

The vector plots of velocity, where the fluid flows across the rods in RBHX and RBXHSCT, are shown in Figs. 3 and 4. As seen in Fig. 3, the vortices are generated in the zones where the fluid flows across the rods. Simultaneously, a number of vortices can be observed near the tube wall. These vortices enchance the heat transfer rate between the fluid and the tubes. This phenomenon is considered the heat transfer enchancement mechanism in RBHX. However, in Fig. 4, we can observe that little vortices were generated when the fluid flows across the rods. In Fig. 5 the path lines of fluid which flow between Rod-baffles in different heat exchangers were given. It can be observed that the path lines between Rod-baffles in RBHX are almost parallel with each other. Meanwhile, the path lines between Rod-baffles in RBHXSCT are much more curved than those in RBHX due to the influence by the spirally corrugated tubes. That is to say, between the Rod-baffles, the fluid in RBHX flow along the

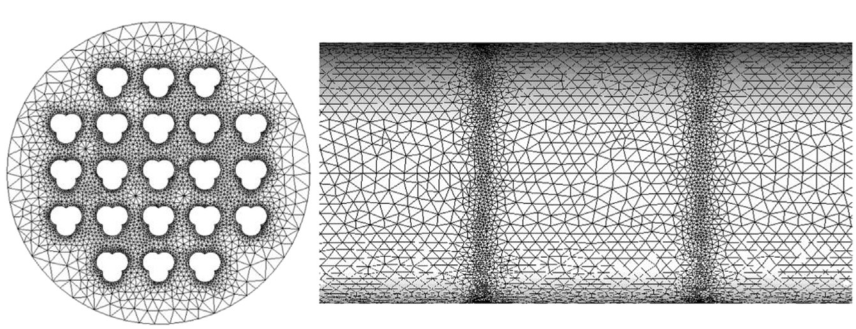

Fig. 2. The mesh of Rod-baffle heat exchanger.

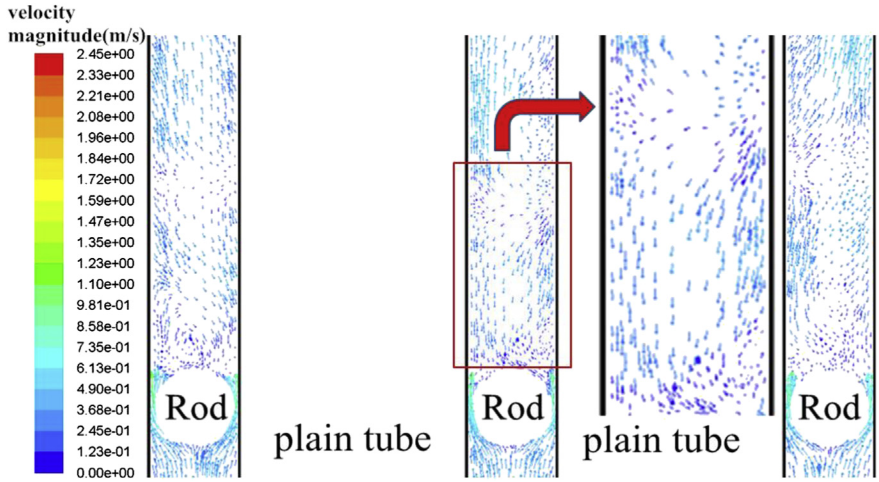

Fig. 3. The velocity vector in Rod-baffle heat exchanger with plain tubes (Re = 18,000).

plain tubes, and the fluid in RBHXSCT is led by the spiral corrugated tubes to flow against the tube wall. The different flow structures between the RBXHSCT and RBHX result in different thermo–hydraulic performances in RBXHsSCT and RBHX, which will be discussed in detail in the following sections.

3.2. Heat transfer

In Fig. 6, the heat transfer performance in terms of the Nusselt numbers of the RBHXsSCT with spirally corrugated tubes are compared with those in RBHX. From this figure, we can see that for each Reynolds number, the Nusselt number increases as the start number of the RBXHSCT decreases. The results show that the Nusselt number in RBHXSCT with one-start spirally corrugated tubes can achieve 287.7, which is 1.2 times than that in RBHX when the Reynolds number is 18,000. Meanwhile, the Nusselt number in RBHX are between those in RBHXsSCT with three–start and four–start spirally corrugated tubes. This phenomenon is caused by the fact that the heat transfer enhancement mechanism in RBHX is caused by the vortices generated near the tube wall when the fluid flows across the rod. In the heat transfer enhancement mechanism in RBHXsSCT, which is different from that in RBHX, fluid is leaded by the spiral flow channels of the spirally corrugated tubes to flow against the tube wall. Fig. 7 shows the plots of velocity fields on cross sections in RBHXsSCT with different start number spirally corrugated tubes when the Reynolds number is 18,000. From this figure, we can observe that as the start number decreases, the warm area becomes larger and the warm degree becomes deeper. Meanwhile, the “red zones” are closer to the tube walls as the start number decreases. That is to say, the velocity gradient becomes larger near the walls. This demonstrate that the lower the start number of the spirally corrugated tubes, the more intense the disturbance to the fluid by the tubes. Therefore, the heat transfer performance in RBHXSCT with one–start spirally corrugated tubes is better than that in other styles of RBHXsSCT and RBHX. The disturbance to the fluid by the tubes is relatively weak in RBHXSCT with four–start spirally corrugated tubes. Thus, the Nusselt numbers in RBHXSCT with four–start spirally corrugated tubes are the least among all the heat exchangers.

Fig. 8 shows the heat transfer quantities in RBHXsSCT and RBHX. Although the Nusselt numbers in RBHXSCT with four-start spirally corrugated tubes are smaller than those in other heat exchangers,

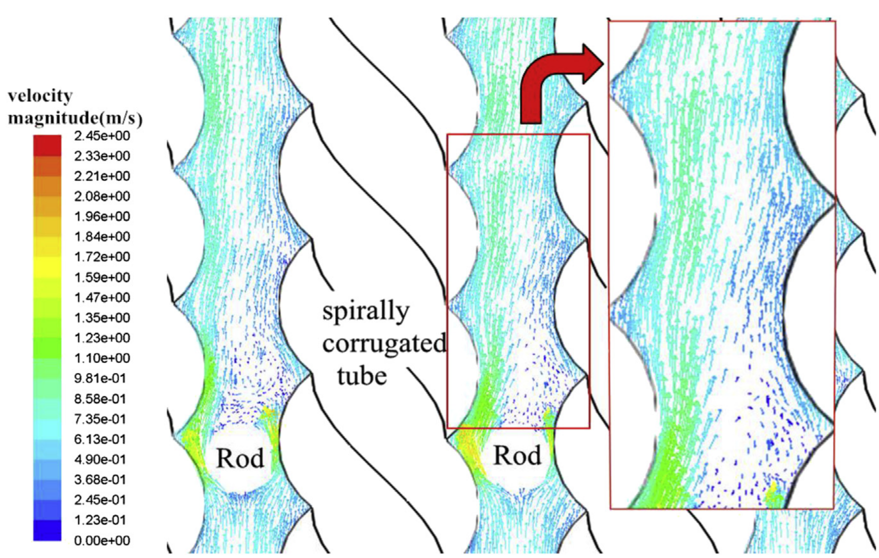

Fig. 4. The velocity vector in Rod-baffle heat exchanger with spirally corrugated tubes (Re = 18000).

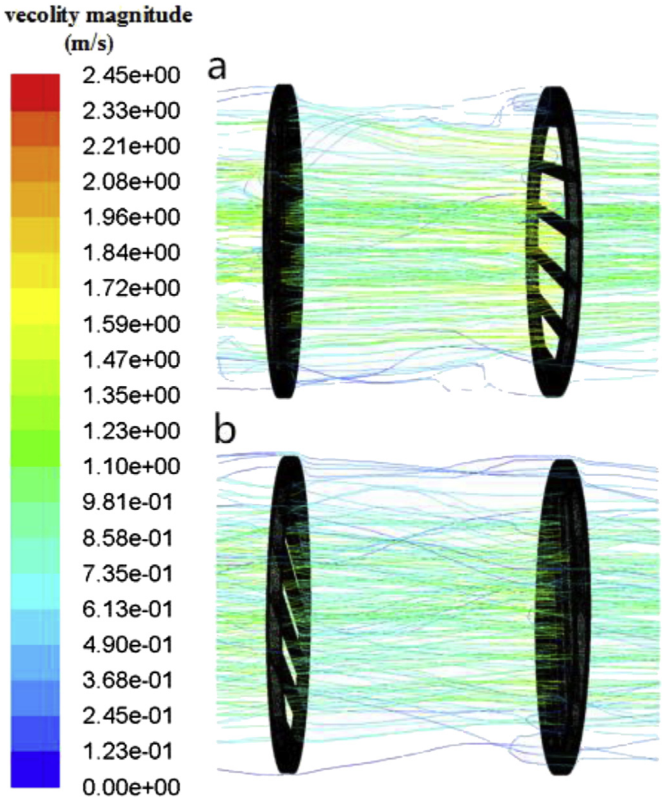

Fig. 5. The path lines in different heat exchangers (Re = 18,000). (a) The path lines in RBHX. (b) The path lines in RBHXSCT with spirally corrugated tubes.

RBHXSCT with four-start spirally corrugated tubes has the largest heat transfer quantities among all heat exchangers. The heat transfer quantities in RBHXsSCT are all larger than those in RBHX. The results show that the heat transfer quantities in the RBHXsSCT with one-start, two-start, three-start, and four-start spirally corrugated tubes are 104.6%, 105.4%, 106.7%, and 109.6%, respectively, higher than that in RBHX. This finding can be attributed to the fact that the higher the start number of the RBHXSCT, the more heat transfer area in the heat exchangers. Although the heat transfer rates are smaller in RBHXsSCT with corrugated tubes with more start number, the total heat transfer quantities in these heat exchangers are larger than those in RBHX.

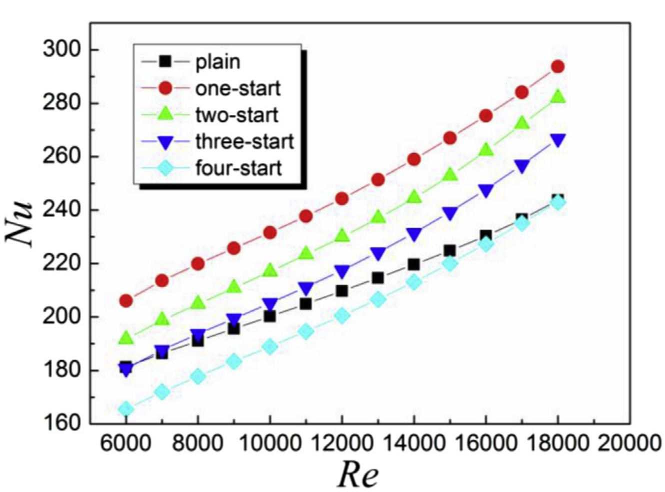

Fig. 6. Variation of Nusselt number with Reynolds number for RBHX and RBHXsSCT.

To illustrate the different thermal performances between the RBHX and RBHXSCT with one-start spirally corrugated tubes, we take a section every 200 mm in those heat exchangers mentioned above and present the temperature field plots of these sections in Fig. 9 when the Reynolds number is 18,000. It is clearly observed that, as the flow develops, the warm areas and temperature levels of temperature fields in RBHXSCT with one-start spirally corrugated tubes are larger than those in RBHX. It demonstrates that in RBHXSCT with one-start spirally corrugated tubes, the heat from heat exchanger tubes transfer into the shell side fluid more easily than that in RBHX which agrees well with the phenomena shown in Fig. 6.

3.3. Pressure drop

Fig. 10 shows the variation of pressure drops with Reynolds number for RBHX and RBHXSCT. In this figure, the pressure drop in RBHX is larger than that in RBHXSCT. Furthermore, for each Reynolds number, the lower the start number of the spirally corrugated tubes in RBHXSCT, the less the pressure drop. The pressure drop in RBHX is 1.21, 1.16, 1.12, and 1.08 times that in RBHXsSCT with one-start, two-start, three-start, and four-start spirally corrugated tubes, respectively. In RBHX, the vortices generated near the tube wall lead to large local resistance loss. However, few vortices are generated in RBHXsSCT; thus, the pressure losses mainly come from the on-way resistance loss, which is less than the local resistance loss. The higher the start numbers of the RBHXSCT, the more spiral flow channels are present in RBHXSCT, and the more disturbance occurs to the fluid. Therefore, the pressure drop in RBHXSCT with one–start spirally corrugated tube is less than that of other RBHXsSCT and RBHX.

Fig. 11 shows the plots of pressure fields in RBHX and RBHXSCT with one -start spirally corrugated tubes which is set as an example when the Reynolds number is 18,000. It is shown that the pressure distributions on the sections of RBHXSCT with one-start spirally corrugated tubes are very homogenous as those in RBHX. Thus, the induced vibration can be prevented effectively in RBHXsSCT which improve the security and reliability of the heat exchangers.

3.4. The overall heat transfer performance

Liu et al. [38] presented the efficiency evaluation coefficient (EEC) in heat transfer process on the basis of the power consumption to describe the heat transfer enchancement degree, which is defined as follows:

$$\mathrm{EEC} = \frac{Q/Q_0}{P/P_0}, \tag{13}$$

where Q and P are the quantity of heat transfer and power consumption in objective equipment, respectively; Q_0 and P_0 are the quantity of heat transfer and power consumption in the comparable equipment, respectively. In this paper, the objective equipment is the RBHXSCT, and the comparable equipment is the RBHX. The power consumption P and P_0 are calculated as in Eqs. (14) and (15):

$$P = v_s \cdot \Delta p_s, \tag{14}$$

$$P_0 = v_0 \cdot \Delta p_0, \tag{15}$$

where v_s and v_0 are the volume flow rate of RBHXSCT and RBHX, respectively; Δp_s and Δp_0 are the pressure drops in RBHXSCT and RBHX, respectively.

According to the Eqs. (13)–(15), it is clearly that EEC is larger than 1 or close to 1, is ideal and applicable for energy-saving purpose as the ratio of heat transfer enhancement is larger than the

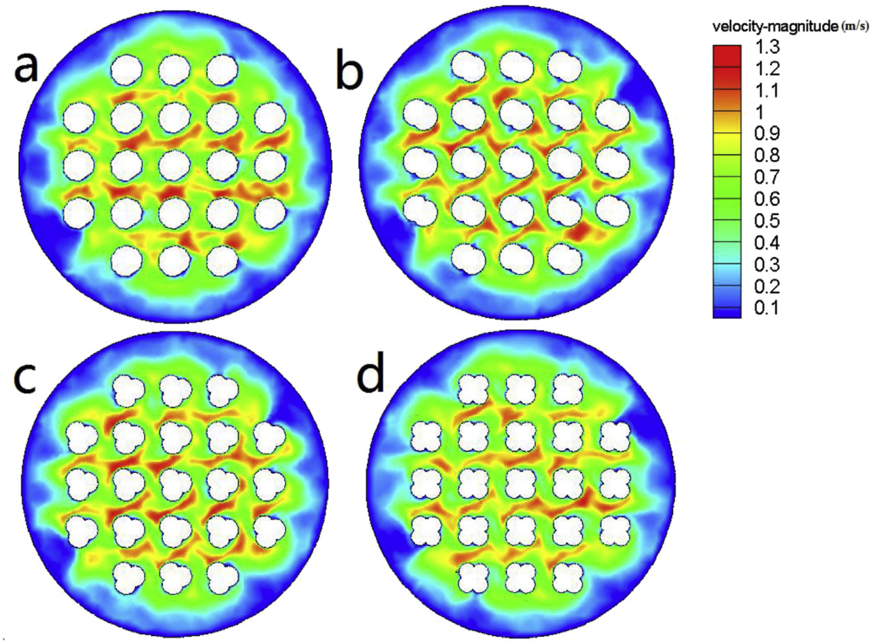

Fig. 7. The plots of velocity fields on cross sections in RBHXsSCT with different start number spirally corrugated tubes (Re = 18000). (a) One-start spirally corrugated tubes. (b) Two-start spirally corrugated tubes. (c) Three-start spirally corrugated tubes. (d) Four-start spirally corrugated tubes.

ratio of power consumption increase. Fig. 12 shows the EEC values in RBHXsSCT with different start numbers. From this picture, we can find that all the EEC values in RBHXsSCT are larger than 1. Thus, compared with the RBHX, the profit (quantity of heat transfer) increase rate is larger than the cost (power consumption) increase rate in RBHXsSCT. This is because the spirally corrugated tubes in heat exchangers influence the shell side fluid, and change the flow condition, which improve the overall thermal performance. The EEC value in RBHXSCT with one–start spirally corrugated tubes can archive 1.35 when the Reynolds number is 18,000, thus making this heat exchanger promising to be widely applied in various industries.

3.5. Physical quantity synergy analysis

Guo [39–41] investigated the physical mechanism of convective heat transfer and proposed field synergy principle to enhance heat transfer, considering the evaluation of convective heat transfer is related to the synergy of velocity and temperature field. Liu et al. [35–37] proved multi–field physical quantity synergy for convective heat transfer by introducing more synergy angles on the basis of velocity field, temperature field, and pressure field and by revealing the fundamental nature of heat transfer enhancement and pressure reduction. The physical nature of enhancing heat transfer and reducing flow resistance, which is directly associated with synergy angles β and θ, is also explained.

The synergy angle between the velocity vector $\vec{U}$ and temperature gradient ∇T of a fluid particle M in the flow field can be written as

$$\beta = \arccos \frac{\vec{U} \cdot \nabla T}{\left|\vec{U}\right| |\nabla T|} \tag{16}$$

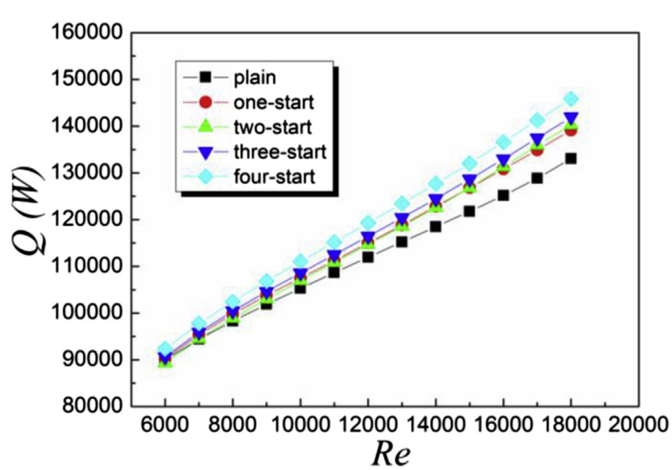

Fig. 8. Variation of the heat transfer quantities with Reynolds number for RBHX and RBHXsSCT.

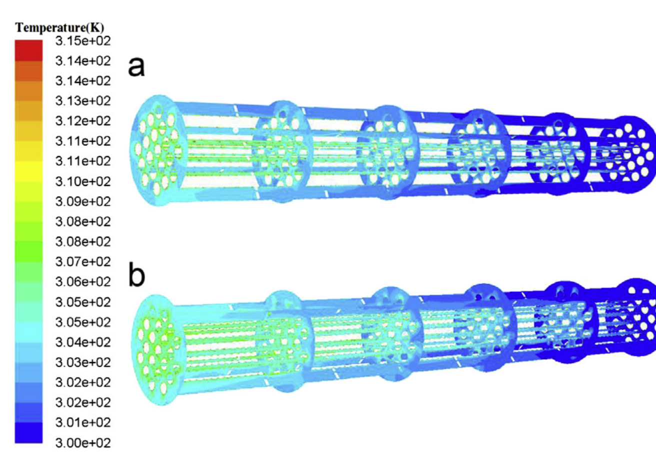

Fig. 9. The plots of temperature fields in different heat exchangers. (a) The plots of temperature fields in RBHX. (b) The plots of temperature fields in RBHXSCT with one-start spirally corrugated tubes.

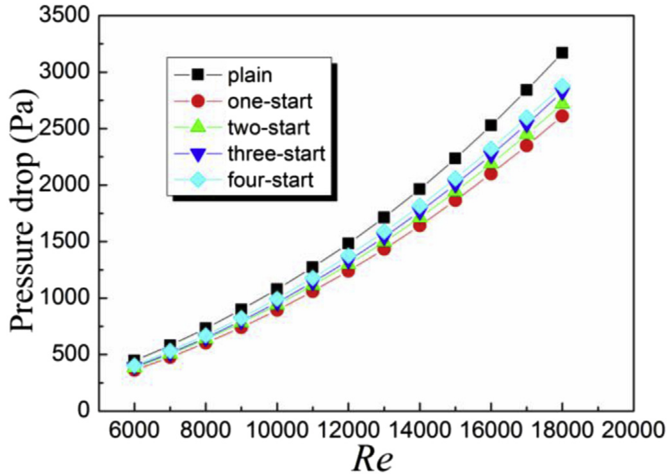

Fig. 10. Variation of pressure drop with Reynolds number for RBHX and RBHXsSCT.

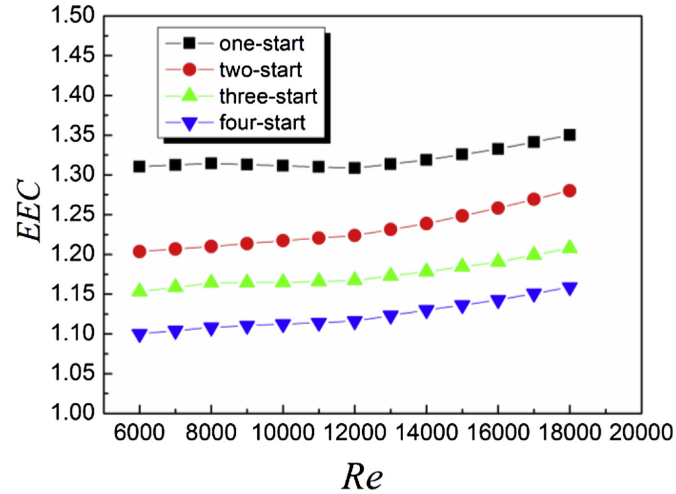

Fig. 12. EEC values of RBHXsSCT on various Reynolds number.

The synergy angle between the velocity vector $\vec{U}$ and pressure gradient ∇p of a fluid particle M in the flow field can be written as

$$\theta = \arccos \frac{\vec{U} \cdot \nabla p}{\left|\vec{U}\right| |\nabla p|} \tag{17}$$

Fig. 13 shows the average synergy angle β for RBHX and RBHXsSCT with different start numbers of the spirally corrugated tubes. As shown in the figure, the average synergy angle β between fluid velocity $\vec{U}$ and temperature gradient ∇T decrease as the start number decreases in the RBHXsSCT at the same Reynolds number, and the β values in RBHX are between those in RBHXsSCT with three-start and four-start spirally corrugated tubes. By observing Fig. 13 we can conclude that the smaller the average synergy angle β, the higher the heat transfer rate is, which is in accordance with the conclusions of [36] and [41].

Fig. 14 shows the average synergy angle θ for RBHX and RBHXsSCT with different start numbers of the spirally corrugated tubes. As shown in the picture, the average synergy angle θ between fluid velocity $\vec{U}$ and pressure ∇p decreases as the start number decreases in the RBHXsSCT at the same Reynolds number, and the θ values in RBHX are the biggest among all heat exchangers. The result shows that the direction of velocity $\vec{U}$ deviates more greatly from the direction of pressure gradient ∇p. Therefore, the synergy between vectors $\vec{U}$ and ∇p should be minimized to design low-resistance heat exchangers.

4. Conclusion

The numerical analysis of heat transfer and fluid flows in the shell sides of the RBHXsSCT and RBHX is carried out, with the aim to improve the overall thermo-hydraulic performance in longitudinal flow heat exchangers. The major findings are summarized as follows:

The velocity vector plots show that in RBHX, the vortices are generated when the fluid flows across the rods. However, in RBHXsSCT, little vortices are generated and the fluid is leaded by the spiral flow channels to flow against the tube walls. The different flow structures between the RBHXsSCT and RBHX result in different thermo–hydraulic performance in these heat exchangers.

The numerical results show that the Nusselt number in RBHXSCT with one-start spirally corrugated tubes can be 1.2 times than that in RBHX when the Reynolds number is 18,000. The heat transfer quantities in the RBHXsSCT with one-start, two-start, three-start, and four-start spirally corrugated tubes are 104.6%,

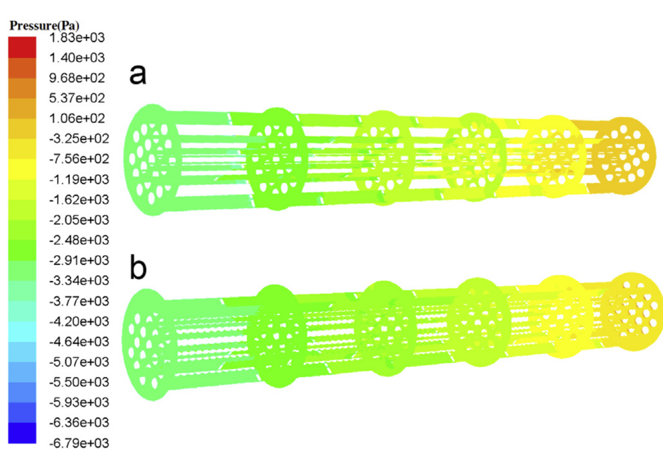

Fig. 11. The plots of pressure fields in different heat exchangers. (a) The plots of pressure fields in RBHX. (b) The plots of pressure fields in RBHXSCT with one-start spirally corrugated tubes.

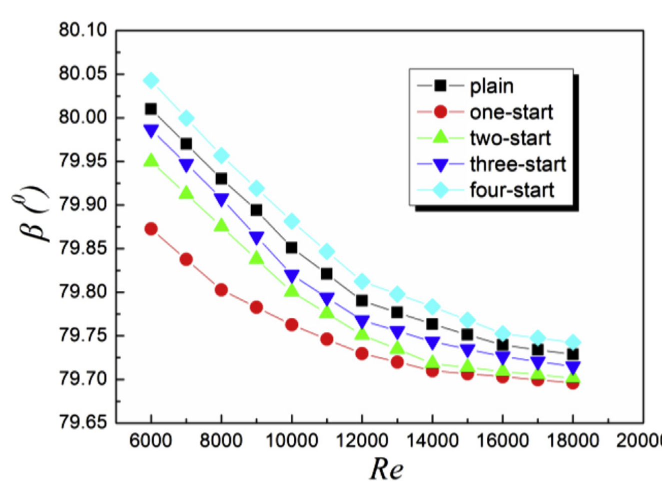

Fig. 13. The β of RBHXsSCT on various Reynolds number.

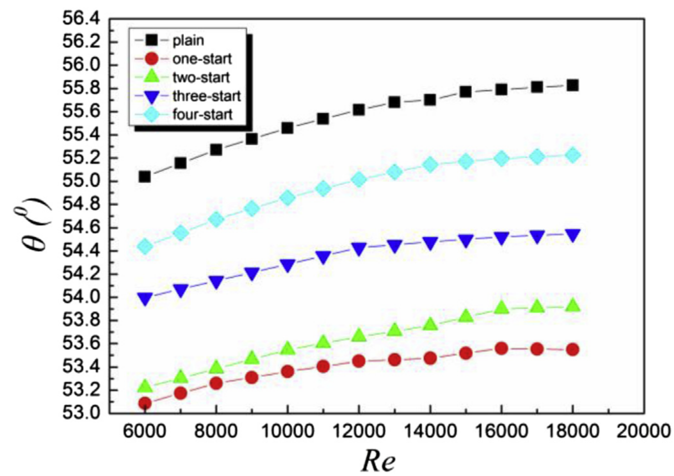

Fig. 14. The θ of RBHXsSCT on various Reynolds number.

105.4%, 106.7%, and 109.6%, respectively, higher than that in RBHX. The pressure drop in RBHX is 1.21, 1.16, 1.12, and 1.08 times than that in RBHXsSCT with one-start, two-start, three-start, and four-start spirally corrugated tubes, respectively. The EEC value in RBHXSCT with one-start spirally corrugated tubes can achieve 1.35, thereby making this heat exchanger promising to be widely applied in various industries.

The physical quantity synergy analysis is performed to investigate the heat transfer and flow resistance performance. The synergy angles β and θ are calculated, and the results verify the synergy regulation among the physical quantities of fluid particles in the flow field of convective. The results of this study can guide us to design an optimum heat exchanger.

Acknowledgments

This work is supported by the National Natural Science Foundation of China (51036003) and the National Key Basic Research Program of China (973 Program) (2013CB228302).

Nomenclature

A_0	the section area of the RBHX (m^2)
A_s	the section area of the RBHXSCT (m^2)
c_p	the specific heat capacity (kJ kg^{-1} K^{-1})
$C_{1\varepsilon}$	empirical constant
$C_{2\varepsilon}$	empirical constant
$C_{3\varepsilon}$	empirical constant
D	the diameter of the shell side in heat exchanger (mm)
D_e	the equivalent diameter for shell side of the heat exchanger (mm)
d_0	the diameter of the plain tubes in RBHX (mm)
d_r	the diameter of the rod (mm)
d_s	the outer diameter of the spirally corrugated tubes in RBHXSCT (mm)
EEC	the efficiency evaluation criteria
G_b	producing item of k by buoyancy (kg m^{-1} s^{-3})
G_k	producing item of k by average velocity gradient (kg m^{-1} s^{-3})
h	heat transfer coefficient (W m^{-2} K^{-1})
k	turbulent kinetic energy (m^2 s^{-2})
M	the mass flux (kg s^{-1})
Nu	the Nusselt number
n	tubes numbers
Δp	shell side pressure drop (Pa)
p_r	rod diameter (mm)
P	power consumption in shell side (J)
Q	the heat transfer quantities in heat exchanger (W)
S	the heat transfer area in heat exchanger (m^2)
S_k	user defined source term (kg m^{-1} s^{-3})
S_ε	user defined source term (kg m^{-1} s^{-4})
Δt_m	logarithmic mean temperature difference (K)
T	fluid temperature (K)
u	fluid velocity in shell side (m s^{-1})
U	fluid velocity vector in general control equation (m s^{-1})
v	volume flow rate (m^3 s^{-1})
x	coordinate axis
y	coordinate axis
Y_M	contribution term from turbulent pulse expansion (kg m^{-1} s^{-3})
z	coordinate axis

Greek symbols

β	synergy angle (°)
θ	synergy angle (°)
λ	thermal conductivity (W m^{-1} K^{-1})
ρ	fluid density (kg m^{-3})
ϕ	universal variable (−)
Γ	generalized diffusion coefficient (−)
ε	turbulent dissipation rate (m^2 s^{-3})
μ	dynamic viscosity (kg m^{-1} s^{-1})
σ_k	Prandtl numbers corresponded to k
σ_ε	Prandtl numbers corresponded to ε

subscripts

i, j	tensor
in	inlet water
k	kinetic energy term
0	RBHX
out	outlet water
s	RBHXSCT
sct	spirally corrugated tubes

References

[1] S.W. Qian, Handbook for Heat Exchanger Design, Chemical Industry Press, Beijing, 2002 (in Chinese).
[2] X.Y. Zhang, Z.C. Liu, W. Liu, Numerical studies on heat transfer and flow characteristics for laminar flow in a tube with multiple regularly spaced twisted tapes, Int. J. Therm. Sci. 58 (2012) 157–167.
[3] J. Guo, A.W. Fan, X.Y. Zhang, et al., A numerical study on heat transfer and friction factor characteristics of laminar flow in a circular tube fitted with center-cleared twisted tape, Int. J. Therm. Sci. 50 (7) (2011) 1263–1270.
[4] J. Guo, Y.X. Yan, W. Liu, et al., Effects of upwind area of tube inserts on heat transfer and flow resistance characteristics of turbulent flow, Exp. Therm. Fluid. Sci. 48 (2013) 147–155.
[5] X.Y. Zhang, Z.C. Liu, W. Liu, Numerical studies on heat transfer and friction factor characteristics of a tube fitted with helical screw-tape without core-rod inserts, Int. J. Heat Mass Transfer 60 (2013) 490–498.
[6] A.W. Fan, J.J. Deng, J. Guo, et al., A numerical study on thermo–hydraulic characteristics of turbulent flow in a circular tube fitted with conical strip inserts, Appl. Therm. Eng 31 (14–15) 2819–2828.
[7] A.W. Fan, J.J. Deng, A. Nakayama, et al., Parametric study on turbulent heat transfer and flow characteristics in a circular tube fitted with louvered strip inserts, Int. J. Heat Mass Transfer 55 (2012) 5205–5213.
[8] Z.F. Huang, A. Nakayama, K. Yang, et al., Enhancing heat transfer in the core flow by using porous medium insert in a tube, Int. J. Heat Mass Transfer 53 (2010) 1164–1174.
[9] W. Liu, K. Yang, Mechanism and numerical analysis of heat transfer enhancement in the core flow along a tube, Sci. China Ser. E Technol. Sci. 51 (8) (2008) 1195–1202.
[10] V.D. Zimparov, N.L. Vulchaanov, L.B. Delov, Heat transfer and friction characteristics of spirally corrugated tubes for power plant condensers, Int. J. Heat Mass Transfer 34 (5) (1991) 2187–2197.

[11] J.A. Meng, X.G. Liang, Z.J. Chen, et al., Experimental study on convective heat transfer in alternating elliptical axis tubes, Exp. Therm. Fluid Sci. 29 (4) (2005) 457–465.
[12] K.J. Bell, Heat exchanger design for the process industries, J. Heat. Transfer Trans. ASME 126 (2004) 877–885.
[13] T. Tinker, Shell side characteristics of shell and tube heat exchangers, parts I, II, III, in: Proceedings of the General Discussion on Heat Transfer, Institution of Mechanical Engineers, London, 1951, pp. 89–116.
[14] J.W. Palen, J. Taborek, Solution of shell side flow pressure drop and heat transfer by stream analysis method, in: CEP Symp. Ser, 1969, pp. 65–92.
[15] J.F. Zhang, Y.L. He, W.Q. Tao, 3D numerical simulation on shell–and–tube heat exchangers with middle-overlapped helical baffles and continuous baffles – Part I: numerical model and results of whole heat exchanger with middle-overlapped helical baffles, Int. J. Heat Mass Transfer 52 (23–24) (2009) 5371–5380.
[16] J.F. Zhang, Y.L. He, W.Q. Tao, 3D numerical simulation on shell-and-tube heat exchangers with middle–overlapped helical baffles and continuous baffles – Part II: simulation results of periodic model and comparison between continuous and noncontinuous helical baffles, Int. J. Heat Mass Transfer 52 (23–24) (2009) 5381–5389.
[17] J.F. Guo, M.T. Xu, L. Cheng, The application of field synergy number in shell-and-tube heat exchanger optimization design, Appl. Energy 86 (2009) 2079–2087.
[18] Y.S. Wang, Z.C. Liu, S.Y. Huang, et al., Experimental investigation of shell-and-tube heat exchanger with a new type of baffles, Heat Mass Transfer 47 (7) (2011) 833–839.
[19] D. Karl, P. Stehlik, R.J. Ploeg, et al., Helical baffles shell-and-tube heat exchangers, Part 1: experimental verification, Heat Transfer Eng. 17 (1996) 93–101.
[20] P. Stehlik, J. Nemcansky, D. Karl, L.W. Swanson, Comparison of correction factors for shell-and-tube heat exchangers with segmental or helical baffles, Heat Transfer Eng. 15 (1994) 55–65.
[21] C.C. Gentry, Rod-baffle heat exchanger technology, Chem. Eng. Prog. 86 (1990) 48–56.
[22] C.C. Gentry, Rod baffle heat exchanger, Appl. Therm. Eng. 18 (1998) VII–VIII.
[23] C.C. Gentry, ROD baffle heat exchanger design and application, in: Proceedings of the Tenth International Heat Transfer Conference: Heat Transfer, Brighton, UK, 1994, pp. 137–142.
[24] R.A. Smyth, A comparative assessment of Rod baffle shell-and-tube heat exchangers, Heat Transfer Eng. 2 (3–4) (1981) 90–94.
[25] L. Ma, Y.S. Wang, J. Yang, et al., Numerical simulation of rod baffle heat exchangers and its optimum design, J. Eng. Thermophys. 32 (3) (2011) 462–464 (in Chinese).
[26] L. Ma, Y.S. Wang, J. Yang, et al., Analysis of flow and heat transfer in rod baffle heat exchangers with rods of variable sections, J. Eng. Thermophys. 33 (1) (2011) 113–116 (in Chinese).
[27] Q.W. Dong, Y.Q. Wang, M.S. Liu, Numerical and experimental investigation of shellside characteristics for Rodbaffle heat exchanger, Appl. Therm. Eng. 28 (7) (2008) 651–660.
[28] Y.S. Wang, Theoretical and Experimental Studies of Fluid Flow and Heat Transfer for Logitudinal Flow Shell-and-tube Heat Exchanger (Ph.D thesis), Huazhong university of science and technology, Wuhan, Hubei, 2011.
[29] K. Yang, W. Liu, Forming an equivalent thermal boundary layer for fully developed laminar tube flow and its field synergy analysis, J. Eng. Thermophys. 28 (2) (2007) 283–285 (in Chinese).
[30] K. Kritikos, C. Albanakis, D. Missirlis, Z. Vlahostergios, A. Goulas, P. Storm, Investigation of the thermal efficiency of a staggered elliptic-tube heat exchanger for aero engine applications, Appl. Therm. Eng. 30 (2010) 134–142.
[31] A.M. Gustafsson, L. Westerlund, G. Hellström, CFD-modeling of natural convection in a groundwater-filled borehole heat exchanger, Appl. Therm. Eng. 30 (2010) 683–691.
[32] N. Tsuzuki, Y. Kato, T. Ishizuka, High performance printed circuit heat exchanger, Appl. Therm. Eng. 27 (2007) 1702–1707.
[33] M.M. Aslam Bhutta, et al., CFD applications in various heat exchangers design: a review, Appl. Therm. Eng. 32 (2012) 1–12.
[34] Y. Wu, G. Gan, A. Verhoef, P.L. Vidale, R.G. Gonzalez, Experimental measurement and numerical simulation of horizontal-coupled slinky ground source heat exchangers, Appl. Therm. Eng. 30 (2010) 2574–2583.
[35] W. Liu, Z.C. Liu, Z.Y. Guo, Physical quantity synergy in laminar flow field of convective heat transfer and analysis of heat transfer enhancement, Chin. Sci. Bull. 54 (19) (2009) 3579–3586.
[36] W. Liu, Z.C. Liu, S.Y. Huang, Physical quantity synergy in the field of turbulent heat transfer and its analysis for heat transfer enhancement, Chin. Sci. Bull. 55 (23) (2010) 2589–2597.
[37] W. Liu, Z.C. Liu, T.Z. Ming, Z.Y. Guo, Physical quantity synergy in laminar flow field and its application in heat transfer enhancement, Int. J. Heat Mass Transfer 52 (19–20) (2009) 4669–4672.
[38] W. Liu, Z.C. Liu, L. Ma, Application of a multi-field synergy principle in the performance evaluation of convective heat transfer enhancement in a tube, Chin. Sci. Bull. 57 (2012) 1600–1607.
[39] Z.Y. Guo, D.Y. Li, B.X. Wang, A novel concept for convective heat transfer enhancement, Int. J. Heat Mass Transfer 41 (14) (1998) 2221–2225.
[40] J. Yang, L. Ma, J. Bock, et al., A comparison of four numerical modeling approaches for enhanced shell-and-tube heat exchangers with experimental validation, Appl. Therm. Eng. 65 (2014) 369–383.
[41] Z.Y. Guo, W.Q. Tao, R.K. Shah, The field synergy (coordination) principle and its applications in enhancing single phase convective heat transfer, Int. J. Heat Mass Transfer 48 (9) (2005) 1797–1807.